



The promotion effect of hydrogen spillover on CH₄ reforming with CO₂ over Rh/MCF catalysts



Linping Qian*, Wenjia Cai, Li Zhang, Lin Ye, Jie Li, Min Tang, Bin Yue*, Heyong He*

Department of Chemistry and Shanghai Key Laboratory of Molecular Catalysis and Innovative Materials, Collaborative Innovation Center of Chemistry for Energy Materials, Fudan University, Shanghai 200433, China

ARTICLE INFO

Article history:

Received 6 June 2014

Received in revised form 5 September 2014

Accepted 6 September 2014

Available online 16 September 2014

Keywords:

Methane

Carbon dioxide

Rh/MCF

Hydrogen spillover

Dry reforming

ABSTRACT

The mesocellular silica foams (MCF) supported rhodium catalysts, prepared by wetness impregnation method, were tested in CH₄ reforming with CO₂. Hydrogen temperature-programmed desorption (H₂-TPD) analysis showed that hydrogen spillover occurs on MCF loaded with highly dispersed rhodium. The turnover frequency of CH₄ (TOF_{CH₄}(s⁻¹)) increased with the strength rise of spilt-over hydrogen. The promotion mechanism was investigated by controlled atmosphere ¹³C and ¹H MAS NMR. The spilt-over hydrogen atoms were found to adsorb on the bridged oxygen sites (Si–O–Si) of MCF and to form surface terminal silanol groups. Meanwhile, in the reforming reaction steps, CH₄ dissociation into CH₃* and CH₃O* decomposition into CH₂O* occurred. The results confirmed that hydrogen atoms can spill over from highly dispersed rhodium species to the neighboring bridged oxygen atoms of MCF, which promotes the reaction by facilitating rate determining steps of CH₄ dissociation and CH_xO* (x = 2, 3) intermediates decomposition on metal surface.

© 2014 Elsevier B.V. All rights reserved.

1. Introduction

CH₄ dry reforming with CO₂ has attracted great attention for the conversion of greenhouse gases, the suitable H₂/CO ratio of the product for Fischer–Tropsch synthesis, and the feasibility in chemical energy transmission systems [1]. A major challenge in the dry reforming process is the lack of the effective catalyst to be able to operate efficiently under severe reaction conditions with good stability. Rhodium-containing catalysts are generally considered to be stable and active in the dry reforming reaction [2–6]. For the reforming catalysts study, metal dispersion [4,5,7,8], metal particle size [6,9–11], and the interaction between metal and support [12–14] were reported to influence the catalytic activity and stability. Wei and Iglesia [4] demonstrated that CH₄ forwards rate is completely independent on the identity of the different support and only depends on the Rh particle size and structure. This conclusion is mainly based on the investigation of the supports of γ-Al₂O₃ and ZrO₂ which were considered to possess weak electric effect on the metal [4]. When strong metal–support interaction (SMSI) occurs on the catalyst such as Rh/TiO₂, TiO_x species can be generated to decorate the metal surface and produce the oxygen to activate the reactants, especially to promote the rate

determining step of CH₄ dissociation through forming CH_xO* intermediates [3,14]. Thus, the turnover rate of the dry reforming reaction is significantly enhanced in comparison with Rh/SiO₂ which has the similar electronic structure of the metal. In addition, when the metal interacts with the support and a direct contact forms, hydrogen atoms adsorbed or generated on the metal may migrate to the acceptor of the support. This phenomenon was called hydrogen spillover [15–23]. Although hydrogen spillover was largely investigated and considered to take part in the hydrogen storage [24–29], hydrogenolysis, hydrogenation, and dehydrogenation reaction [15,20–23,30–41], the mechanism of hydrogen spillover attending the reaction process has not been illustrated in detail. Collins et al. considered that the spilt-over hydrogen hampers both CH₃OH decomposition and CO production steps in the methanol synthesis via CO₂ hydrogenation over Pd/Ga₂O₃ catalyst [42]. Makkee et al. proposed that the catalytic activity of the dehydrogenation of ethylbenzene to styrene can be influenced greatly by the hydrogen spillover because the dehydrogenation step in this redox system was considered as the dominant route [43]. Therefore, the promotion effect of hydrogen spillover might be disclosed if the direct relationship between the spilt-over hydrogen and the dehydrogenation steps in the dry reforming reaction were confirmed effectively.

The mechanism study of the CH₄ dry reforming reaction is mainly based on the analysis of gas-phase kinetic data and the intermediates formed on the catalysts [44–47]. But one problem occurs in tracking the intermediates evolution due to the limited trap of

* Corresponding authors. Fax: +86 21 65643140.

E-mail addresses: lpqian@fudan.edu.cn (L. Qian), yuebin@fudan.edu.cn (B. Yue), heyonghe@fudan.edu.cn (H. He).

adsorbed species at high reaction temperature. The other is the lack of the strong detection or discrimination of the anchoring way of the spilt-over hydrogen on the support at the same time [48–51]. The *in situ* ^{13}C and ^1H MAS NMR spectroscopy under controlled atmosphere is a powerful technique in the study of intermediates with unique quantitative advantage [52–54]. In our previous work, both H-containing reactive intermediates (CH_xO^* , $2 \leq x \leq 3$) on metal surface and spilt-over hydrogen forming hydroxyls (OH) on the support were observed on Rh/SBA-15 in the dry reforming reaction by controlled atmosphere ^1H MAS NMR technique [53]. Through the quantitative analysis, we proved that the adsorbed CH_4 on Rh surface decomposes into CH_3^* and H^* , the spilt-over latter forms surface hydroxyl group with the bridged oxygen sites (Si–O–Si) of the support. Similar phenomenon about Si–OH formed from hydrogen spillover was observed in hydrogen adsorption on Pt/SiO₂ [51] and partial oxidation of methane on Rh/SiO₂ [55] through *in situ* DRIFTS and FT-IR investigation.

In the present work, an aerogel-like mesoporous material mesocellular silica foam (MCF) with large surface area and remarkable diffusion characteristic [56] was used as the support, which may behave as HMS and SBA-15 to accept the spilt-over hydrogen atoms [19,53] and to enhance the dry reforming reaction. MCF-supported rhodium catalysts with different Rh content were prepared by wetness impregnation method. During the investigation of the dry reforming reaction, the strong hydrogen spillover and the high turnover frequency of CH_4 ($\text{TOF}_{\text{CH}_4}(\text{s}^{-1})$) were found on the catalysts with highly dispersed rhodium species. By controlled atmosphere MAS NMR, the formation of spilt-over hydrogen and the evolution of the intermediates can be obtained simultaneously. After that, the promotion mechanism of hydrogen spillover was further disclosed.

2. Experimental

2.1. Preparation of the catalysts

MCF was prepared according to the literature method [56,57]. Pluronic P123 triblock copolymer ($\text{EO}_{20}\text{PO}_{70}\text{EO}_{20}$, Aldrich) was dissolved in aqueous HCl (2 mol L^{-1}) at room temperature and 1,3,5-trimethylbenzene (TMB) was added. After heating for 45 min at 313 K, tetraethyl orthosilicate (TEOS) was added. The cloudy mixture with an $\text{EO}_{20}\text{PO}_{70}\text{EO}_{20}:\text{TEOS}:\text{HCl}:\text{TMB}$ molar ratio of 4:210:1200:170 was kept at 368 K for 24 h. The precipitate product was filtered and dried, then calcined at 773 K for 8 h in air. The catalysts containing 0.5, 1.0, 2.0, and 3.0 wt% of Rh were prepared by impregnating MCF with desired volume of $\text{RhCl}_3 \cdot 3\text{H}_2\text{O}$ solution (0.20 mol L^{-1}). After drying under an infrared lamp, the catalyst was calcined in air at 573 K for 30 min and then reduced in H_2 at 723 K for 60 min. The samples are denoted to $x \text{ wt\% Rh/MCF}$, where x represents the Rh content.

2.2. Characterization of the catalysts

Small-angle X-ray scattering (SAXS) experiments were performed on a Bruker NanoSTAR U SAXS system equipped with high-resolution pinhole chamber using $\text{Cu-K}\alpha$ radiation ($\lambda = 0.15418 \text{ nm}$). Wide-angle X-ray diffraction (XRD) patterns were recorded using a Rigaku D/MAX-IIA diffractometer with $\text{Cu-K}\alpha$ radiation ($\lambda = 0.15418 \text{ nm}$). Surface area measurements were based on N_2 adsorption data obtained using a Micromeritics Tristar-3000 apparatus at 77 K. The samples were pretreated at 573 K under vacuum for 3 h before N_2 adsorption. The surface area was calculated by the BET method, and the pore size distribution was evaluated by the BJH model. Transmission electron microscopy (TEM) measurements were performed on a JEOL JEM-2011 transmission electron

microscope. Prior to the measurements, the samples were mounted on carbon-coated copper grid by drying a droplet of a suspension of the ground sample in ethanol on the grid.

The dispersion of rhodium was analyzed by the temperature-programmed desorption of H_2 (H_2 -TPD). After being heated at 723 K for 60 min under Ar, the catalyst was cooled to 293 K. Then H_2 was introduced by the pulse method at 293 K until saturation, followed by purging with Ar to remove any gaseous and/or physisorbed H_2 until the thermal conductivity detector (TCD) signal returned to the baseline. The H_2 desorption curves were acquired at a heating rate of 20 K min^{-1} from room temperature to 1073 K. The dispersion of rhodium was calculated based on the area of hydrogen desorption from metal surface with the assumption of $\text{H}:\text{Rh}_{(\text{surface})}$ stoichiometry of 1:1 [58].

Following the first H_2 -TPD, the catalyst of 0.5 wt% Rh/MCF was re-reduced in H_2 at 723 K for 60 min and cooled to room temperature in H_2 . A second H_2 -TPD to 1073 K was obtained as described above [21].

2.3. CH_4 dry reforming with CO_2

The dry reforming experiments at high temperature were conducted at atmospheric pressure in a conventional flow apparatus using a stainless fixed bed reactor with quartz lining. The reactor (i.d. = 3 mm) was electrically heated in a furnace. Typically, 40 mg of 60–80 mesh catalyst was activated in nitrogen at 1023 K for 3 h before reaction. The reaction was carried out at 1023 K with a gas hourly space velocity (GHSV) of $13,500 \text{ mL h}^{-1} \text{ g}_{\text{cat}}^{-1}$ and a $\text{N}_2:\text{CH}_4:\text{CO}_2$ flow rate ratio of 3:1:1. The TOF of CH_4 test was taken at 1023 K with a high GHSV of $120,000 \text{ mL h}^{-1} \text{ g}_{\text{cat}}^{-1}$. The effluent was analyzed using an on-line gas chromatography (GC-122, Shanghai Precision & Scientific Instrument Co., Ltd.) with a TCD. A TDX-01 column was used for the separation of H_2 , CO, CH_4 , and CO_2 . The conversions of CH_4 and CO_2 , the ratio of CO/H_2 , and the TOF of CH_4 are defined as follows:

$$\text{Conv. of } \text{CH}_4 (\%) = \frac{(\text{CH}_4)_{\text{in}} - (\text{CH}_4)_{\text{out}}}{(\text{CH}_4)_{\text{in}}} \times 100,$$

$$\text{Conv. of } \text{CO}_2 (\%) = \frac{(\text{CO}_2)_{\text{in}} - (\text{CO}_2)_{\text{out}}}{(\text{CO}_2)_{\text{in}}} \times 100,$$

$$\text{H}_2/\text{CO} = \frac{(\text{H}_2)_{\text{out}}}{(\text{CO})_{\text{out}}}$$

$$\text{TOF}_{(\text{CH}_4)} = \frac{(\text{CH}_4)_{\text{in}} - (\text{CH}_4)_{\text{out}}}{22400 \times 60 \times m},$$

where $(\text{CO}_2)_{\text{in}}$ and $(\text{CH}_4)_{\text{in}}$ are inlet flow rates (mL/min), $(\text{CO}_2)_{\text{out}}$, $(\text{CH}_4)_{\text{out}}$, $(\text{H}_2)_{\text{out}}$, and $(\text{CO})_{\text{out}}$ are outlet flow rates (mL/min), and m is the molar amount of the active centers determined by H_2 -TPD.

2.4. Controlled atmosphere ^{13}C and ^1H MAS NMR studies

The typical controlled atmosphere ^{13}C and ^1H MAS NMR experiments were similar to those reported in our previous work [53]. About 20 mg of powdered catalyst was packed into a well-balanced quartz cell. Then, the cell was heated at 573 K for 3 h under vacuum condition and then cooled down to room temperature. Total 1–3 molecules of ^{13}C -labeled substance per surface metal atom were dosed through cooling the cell in liquid nitrogen. ^1H -decoupling ^{13}C MAS NMR measurements were carried out on a Bruker Avance DSX300 spectrometer operating at 75.45 MHz with a 90° pulse and a 10 s recycle delay at a spinning rate of ca. 1 kHz. The single pulse ^1H MAS NMR spectra were taken at the same conditions except for the resonance frequency of 300 MHz and the recycle delay of 5 s. Both

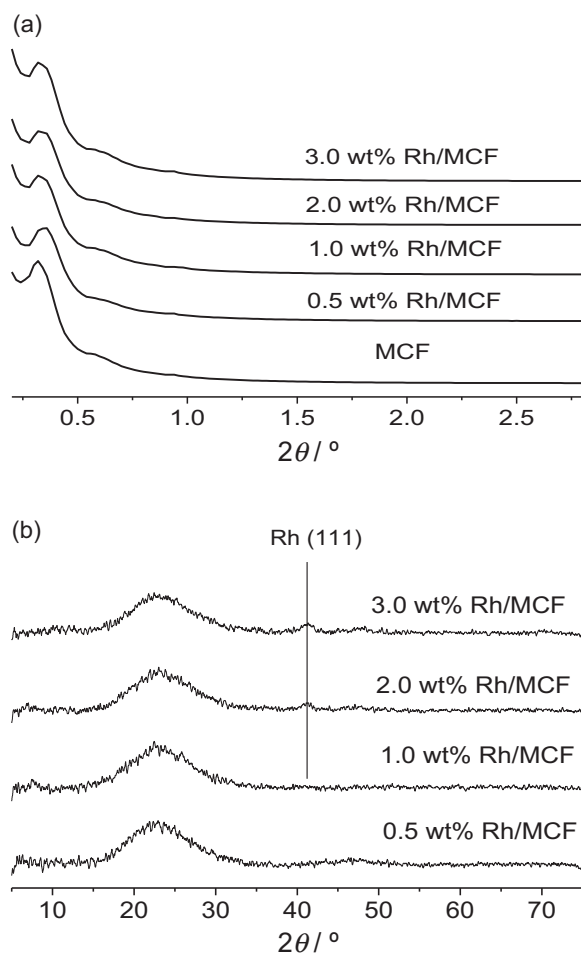


Fig. 1. Small-angle X-ray scattering (a) and XRD (b) patterns of the catalysts.

^{13}C and ^1H chemical shifts were referenced to tetramethylsilane (TMS) as the external standard.

3. Results and discussion

3.1. Catalysts Characterization

Rh/MCF catalysts with rhodium content from 0.5 to 3.0 wt% were characterized by the measurements of SAXS, XRD, TEM, N_2 -sorption, and H_2 -TPD. Fig. 1(a) shows the SAXS data for the Rh/MCF samples and exhibits one strong peak and two higher-order weak peaks which indicate the narrow size distribution of the spherical cells [56,57]. XRD patterns (Fig. 1(b)) of Rh/MCF catalysts show the broad peaks around 2θ of $15\text{--}30^\circ$ which are ascribed to the amorphous silica. Another peak at 41° attributed to the diffraction of Rh(111) was found over Rh/MCF catalysts with Rh loading ≥ 2.0 wt% [59]. It is indicated that rhodium species is highly dispersed on the support over the catalysts with low Rh content (≤ 1.0 wt%).

The porosity of the Rh/MCF was investigated by N_2 -sorption analysis (Fig. 2). The isotherms are of type IV and show type H1 hysteresis at relative high pressures, which is typical for mesoporous materials that not only exhibit capillary condensation and evaporation but also have large pore sizes with narrow size distributions. The pore size analysis according to the modification method suggested by Stucky et al. shows that the cell sizes could be derived from the adsorption branches and the window sizes from the desorption branches [56,57]. The BET surface area, pore size

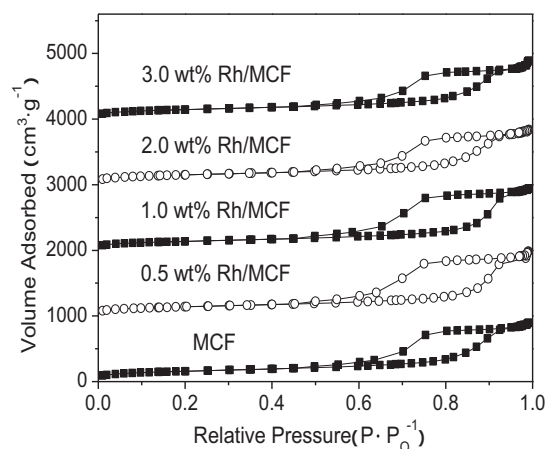


Fig. 2. Nitrogen adsorption-desorption isotherms of the MCF and catalysts.

and pore volume of all calcined samples are presented in Table 1. The surface area, pore size, and pore volume of MCF decrease with rhodium species impregnating, indicating that the rhodium addition may partially block the windows of MCF.

TEM images of Rh/MCF in Fig. 3 reveal a disordered array of silica struts comprising uniformly sized spherical cells (20–34 nm) interconnected by windows, which is characteristic structural feature of the MCF materials [56,57]. Rhodium particles were detected over 3.0 wt% Rh/MCF, indicating that metal particles tend to congregate with more loading.

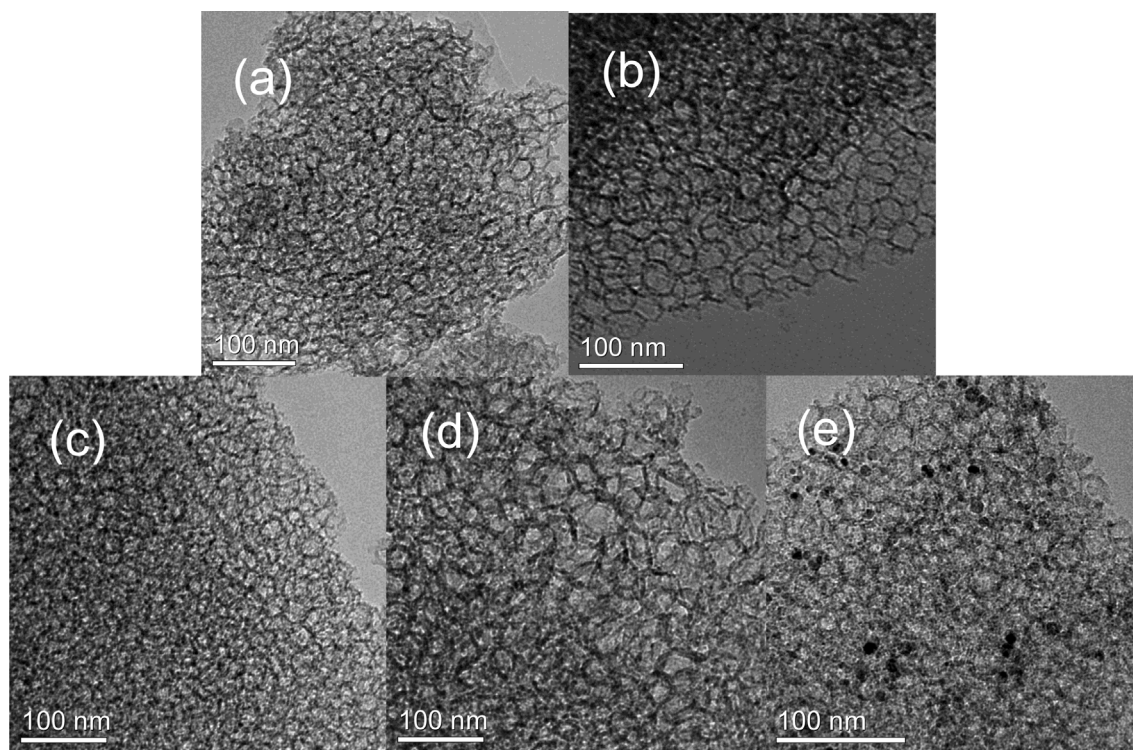
In Fig. 4, H_2 -TPD analysis shows the different adsorption sites for hydrogen (Fig. 4). The silica support of MCF does not adsorb hydrogen. For Rh/MCF catalysts, two hydrogen desorption peaks I and II were observed at around 350 and 700 K. Peak I is attributed to desorbed hydrogen from the metal surface [19,21,41,60,61]. The intensity of peak I does not significantly decrease and the desorption temperature of peak II is much higher than peak I, which indicates no occurrence of the strong metal-support interaction and hydrogen chemisorbed at metal-support interface [17,62]. Peak II is attributed to desorption of the spilt-over hydrogen [19,21,41,60,61]. The chemisorption of hydrogen on metal surface is considered to be reversible while the spillover hydrogen is irreversible during the consecutive H_2 -TPD process [21]. Thus, the chemisorbed hydrogen on metal can be disclosed in H_2 -TPD analysis following the first. The second H_2 -TPD profile of 0.5 wt% Rh/MCF in Fig. 4 clearly shows the chemisorbed hydrogen on metal desorbs around 350 K and no obvious desorption around 700 K. The estimation of rhodium dispersion is based on the desorption area of peak I with the assumption of $\text{H}:\text{Rh}_{\text{surface}}$ stoichiometry of 1:1. The rhodium dispersion and the corresponding metal loading are presented in Fig. 5(a). It is noticeable that the metal dispersion decreases with a rise of rhodium loading, indicating that rhodium species begins to congregate with more metal impregnated. The relationship of hydrogen spillover with metal dispersion was shown in Fig. 5(a). The strength of hydrogen spillover calculated by spilt-over hydrogen per surface rhodium atom ($\text{Area}_{\text{peak(II)}}/\text{Area}_{\text{peak(I)}}$ in Fig. 4) increases with the increment of metal dispersion (Fig. 5(a)). It indicates that highly dispersed rhodium species could interact with the MCF support strongly to form the anchored interface due to its large occurrence of coordinately unsaturated metal sites [3–6,63], which might benefit hydrogen atom to spill over from metal to support greatly.

3.2. Catalytic performance

The effects of the reaction temperature and rhodium loading on the catalytic activity over Rh/MCF are shown in Fig. 6. With

Table 1N₂ sorption analysis of MCF and Rh/MCF.

Samples	Cell diameter ^a	Window diameter ^a	BET surface area (m ² g ⁻¹)	Pore volume (cm ³ g ⁻¹)
MCF	22.7	7.1	656	1.7
0.5 wt% Rh/MCF	22.5	6.9	555	1.5
1.0 wt% Rh/MCF	22.4	6.9	545	1.5
2.0 wt% Rh/MCF	21.6	6.6	539	1.5
3.0 wt% Rh/MCF	21.5	6.5	522	1.4

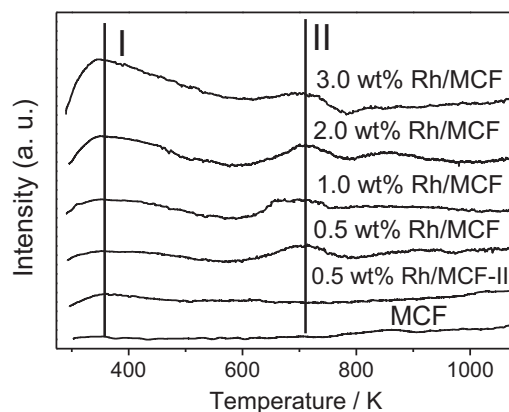
^a Determined from N₂ sorption by the BJH model.**Fig. 3.** TEM images of (a) 0.0 wt% MCF, (b) 0.5 wt% Rh/MCF, (c) 1.0 wt% Rh/MCF, (d) 2.0 wt% Rh/MCF, and (e) 3.0 wt% Rh/MCF.

increasing temperature, the conversions of CH₄ and CO₂ increase. The conversions of CO₂ are slightly higher than those of CH₄ and the ratios of H₂/CO are slightly lower than one unit. This phenomenon could be explained by the occurrence of reverse water gas shift reaction, $\text{H}_2 + \text{CO}_2 \rightarrow \text{H}_2\text{O} + \text{CO}$ [3,5]. With increasing rhodium loading from 0.5 to 3.0 wt%, the conversions of CH₄ and CO₂ reach a maximum over 2.0 wt% Rh/MCF catalyst. The stability of the catalysts

is shown in Fig. 7. No significant loss of the catalytic activity was detected during the dry reforming reaction test of 100 h. It is indicated that Rh/MCF catalysts possess high catalytic stability in the dry reforming of CH₄ with CO₂. The BET surface area of the used samples decreases about 35%. This may be attributed to some carbon species deposition or partial collapse of the catalyst framework [6,64]. But the SAXS and TEM analysis in the Fig. S1 and Fig. S2 show that the structure of the used catalysts is well maintained after the stability test, indicating high thermal stability of Rh/MCF even at severe reaction conditions.

3.3. Effect of rhodium dispersion on the catalytic activity

The relationship between TOF_{CH₄} and rhodium dispersion could be obviously seen in Fig. 5(b). TOF_{CH₄} increases with the increment of rhodium dispersion, especially when rhodium dispersion is above 50%. Total 1.0 wt% Rh/MCF with rhodium dispersion of 61% possesses high spilt-over hydrogen per surface rhodium atom of 1.17 and high TOF_{CH₄} of 3.58. For $\gamma\text{-Al}_2\text{O}_3$ - and ZrO₂-supported rhodium catalysts investigated by Wei and Iglesia [4], the reported work showed that the amount of spilt-over hydrogen for these catalysts is not as large as Rh/MCF (for Rh/ZrO₂ not presented clearly [62], for Rh/ $\gamma\text{-Al}_2\text{O}_3$ with Rh dispersion of 92% spilt-over hydrogen/surface rhodium atom = 0.51 [17]). The catalytic test showed a nearly linear relationship between CH₄ forwards rate and rhodium dispersion (but somewhat low at the high rhodium dispersion more

**Fig. 4.** H₂-TPD profiles of MCF and Rh/MCF samples (0.5 wt% Rh/MCF-II denotes the second H₂-TPD analysis of 0.5 wt% Rh/MCF).

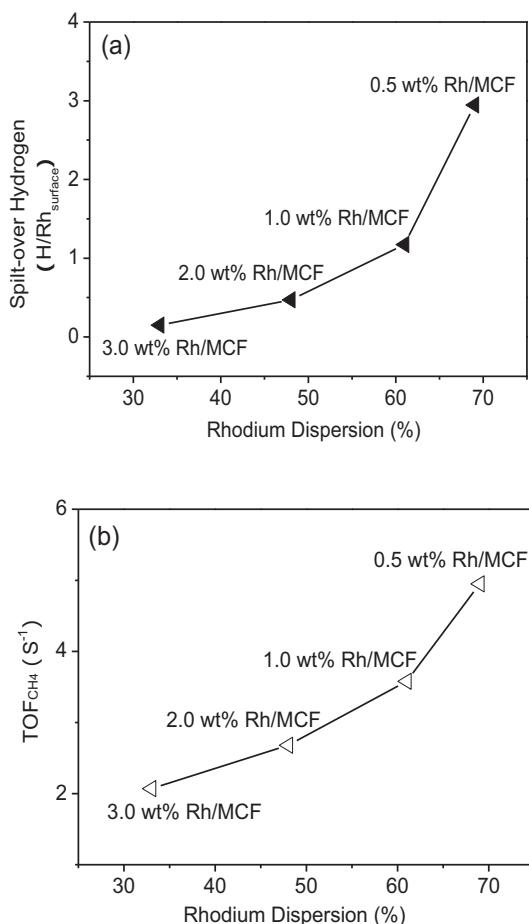


Fig. 5. Effect of rhodium dispersion on (a) the spilt-over hydrogen and (b) TOF_{CH_4} (s^{-1}) over Rh/MCF catalysts.

than 50%), which is considered to be only dependent on rhodium dispersion [4]. But this dependence does not repeat on Rh/MCF completely, especially at high rhodium dispersion CH_4 turnover rate in Fig. 5(b) rises significantly above the line only dependent on metal dispersion simulated according to $Rh/\gamma-Al_2O_3$ and Rh/ZrO_2 [4], which indicates the large occurrence of the extra promotion on the highly dispersed rhodium species. This increment should be attributed to hydrogen spillover on Rh/MCF determined by H_2 -TPD analysis. According to the literature reports [15,20–23], the hydrogenolysis, hydrogenation, and dehydrogenation reaction can be significantly enhanced by hydrogen spilling over from active centers to neighbor sites. Therefore, the dry reforming reaction might be promoted by hydrogen spillover through facilitating the dehydrogenation steps in reforming process such as CH_4 dissociation and the intermediates CH_xO^* decomposition on the active centers which were considered as the rate determining steps [3,4,46]. Further investigation about hydrogen spillover promotion mechanism in CH_4 reforming with CO_2 was carried out by controlled atmosphere MAS NMR in the following section.

3.4. Controlled atmosphere ^{13}C MAS NMR study

Fig. 8 shows ^{13}C MAS NMR spectra of $^{13}CH_4 + ^{12}CO_2$ over 1.0 wt% Rh/MCF after the treatment at different temperature for 30 min consecutively. At room temperature, no reaction occurs. When the temperature increases to 673 K, a new peak appears around 125 ppm which is ascribed to $^{13}CO_2$. With the temperature rising to 773 K, the intensity of $^{13}CO_2$ increases ($^{13}CO_2/^{13}CH_4 \approx 1$)

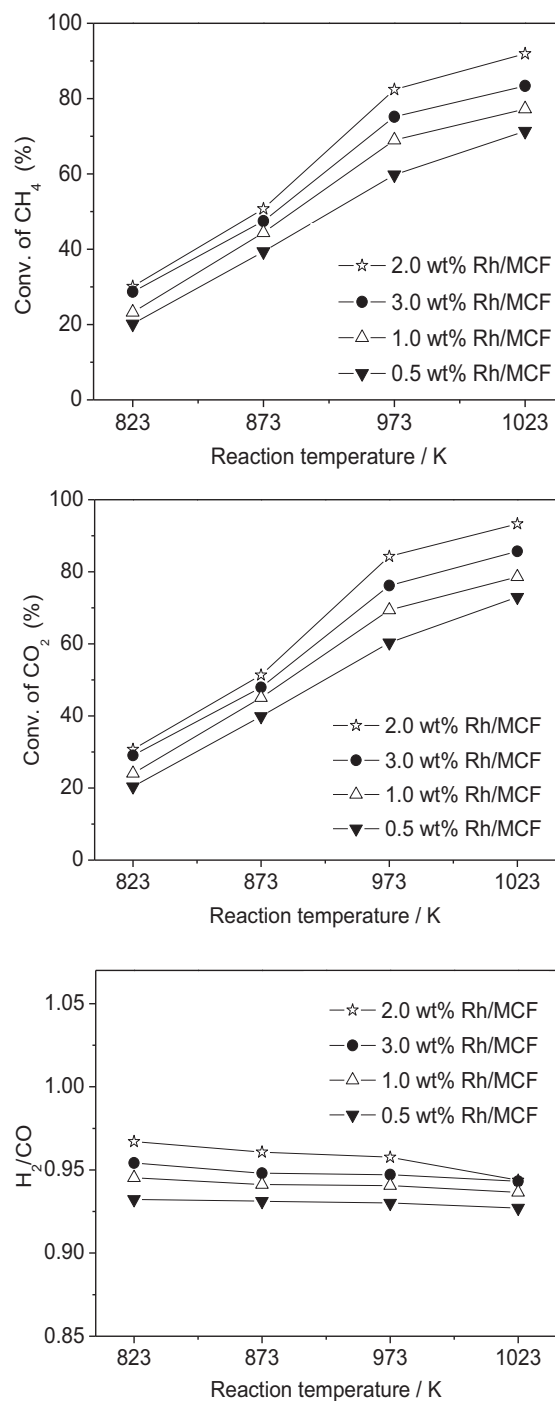


Fig. 6. Effect of reaction temperature on the conversions of CH_4 and CO_2 and the ratio of H_2/CO over Rh/MCF catalysts (GHSV = $13,500 \text{ mL h}^{-1} \text{ g}_{\text{cat}}^{-1}$).

but no signal of ^{13}CO can be observed, indicating the occurrence of the carbon exchange between methane and carbon dioxide ($^{13}CH_4 + ^{12}CO_2 \leftrightarrow ^{12}CH_4 + ^{13}CO_2$) [65] before the dry reforming reaction begins. After heating at 873 K for 30 min, the weak signal of ^{13}CO at 181 ppm was detected, indicating the start of the dry reforming reaction ($CH_4 + CO_2 \rightarrow 2CO + 2H_2$). However, the intermediates in the dry reforming reaction were not observed.

The quantitative analysis of the ^{13}C -labeled substance is shown in Fig. 9. About 37% of $^{13}CH_4$ adsorbed on rhodium surface at room temperature could not be detected due to the Knight shift effect [66]. With increasing temperature, the amount of $^{13}CH_4$ decreases

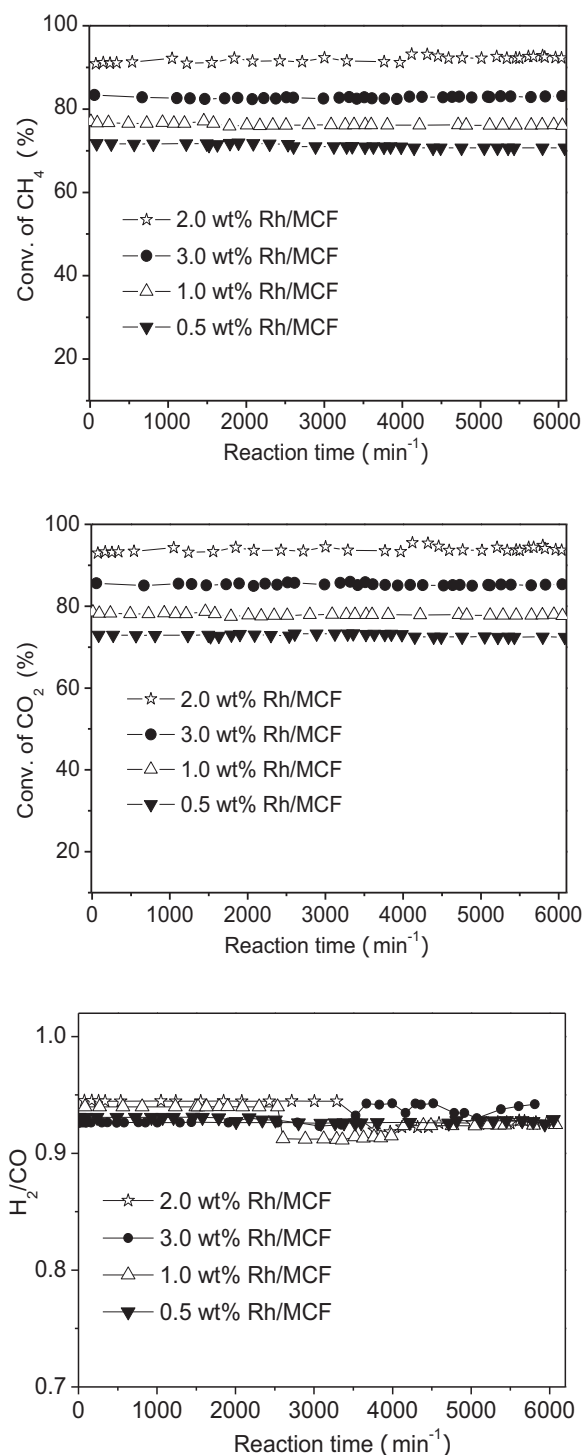


Fig. 7. The catalytic stability in the CH_4 reforming with CO_2 over Rh/MCF catalysts at 1023 K (GHSV = $13,500 \text{ mL h}^{-1} \text{ g}_{\text{cat}}^{-1}$).

while $^{13}\text{CO}_2$ increases due to the occurrence of the carbon exchange reaction, $^{13}\text{CH}_4 + ^{12}\text{CO}_2 \rightarrow ^{12}\text{CH}_4 + ^{13}\text{CO}_2$. When the temperature increases to 773 K, the intensity ratio of $^{13}\text{CH}_4/^{13}\text{CO}_2$ reaches about one unit for the balance of the carbon exchange reaction. In the high temperature range of 873–973 K, the total amount of ^{13}C observed by ^{13}C NMR is increased. This phenomenon could be explained by the competitive adsorption of H_2 produced from the dry reforming reaction against ^{13}C -labeled species on rhodium surface.

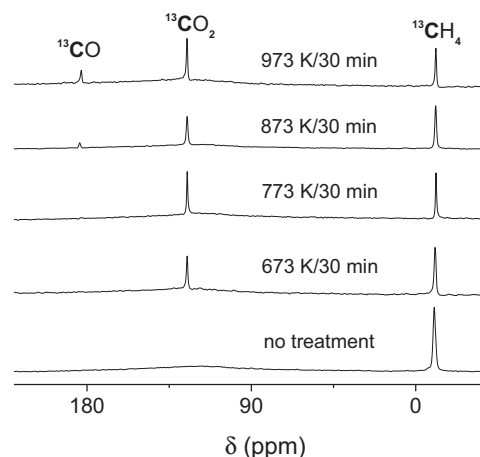


Fig. 8. Controlled atmosphere ^{13}C MAS NMR spectra of the system of $^{13}\text{CH}_4 + \text{CO}_2$ over 1.0 wt% Rh/MCF treated under different temperatures for 30 min consecutively.

3.5. Controlled atmosphere ^1H MAS NMR

In order to obtain the information on the intermediates which cannot be observed in ^{13}C NMR due to the Knight shift effect from rhodium surface, the reactant system of $^{13}\text{CH}_4 + ^{12}\text{CO}_2$ was investigated by ^1H MAS NMR (Fig. 10). At room temperature, the signals of 0.2 and -0.2 ppm are ascribed to the split ^1H signals of CH_4 by the J -coupling of $^{13}\text{C}-\text{H}$. The weak signals of 1.0 and 1.4 ppm are attributed to two types of parent terminal silanol groups of the MCF support [53,67–69]. The quantitative analysis shows that about 26% of total hydrogen could not be detected due to the Knight shift effect of rhodium surface at room temperature. Considering the C:H molar ratio of 1:4 in methane, it is concluded that 37% of the total CH_4 molecules adsorb on rhodium surface through the most adsorption way, i.e., one carbon and three hydrogen atoms attach closely to the rhodium particle at room temperature, because the atom ratio of the adsorbed hydrogen to carbon calculated is 2.8. When the temperature rises to 773 K, the peak around 2.8 ppm appears, ascribing to the spilt-over hydrogen adsorbed on Si–O–Si of the support [69,70]. To confirm the occurrence of this spilling process, the H_2 -treated 1.0 wt% Rh/MCF prior to H_2 -TPD analysis was investigated by NMR and showed a ^1H signal around 2.8 ppm. The amount of spilt-over hydrogen on Si–O–Si equals to ca. 10% of the total amount of hydrogen atoms, which means 40% of the total added CH_4 molecules associated with spilt-over hydrogen. Taking into account 37% of the ‘unobserved’ CH_4 by ^{13}C MAS

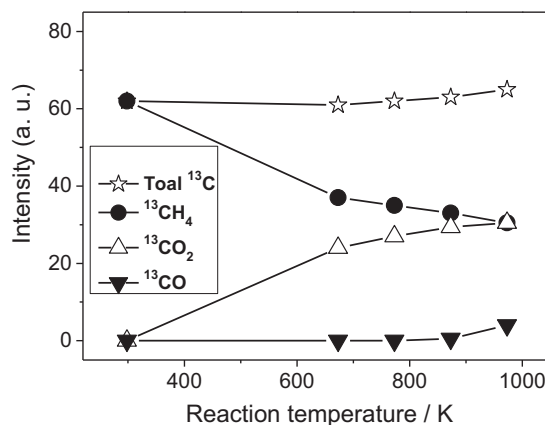


Fig. 9. The quantitative analysis of the ^{13}C -labeled substance in the system of $^{13}\text{CH}_4 + \text{CO}_2$ over 1.0 wt% Rh/MCF at different reaction temperature for 30 min consecutively.

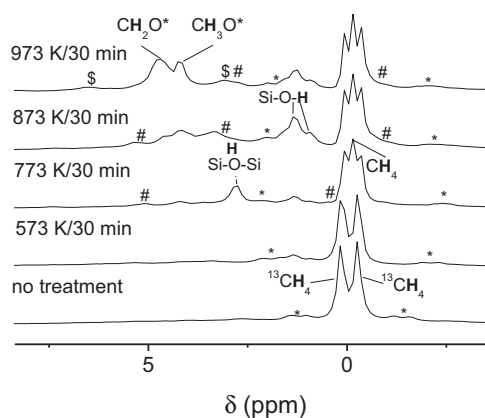


Fig. 10. Controlled atmosphere ^1H MAS NMR spectra of the systems of $^{13}\text{CH}_4 + \text{CO}_2$ over 1.0 wt% Rh/MCF treated under different temperatures for 30 min consecutively. *, #, and \$ denote the spinning sidebands of CH_4 , hydroxyls or hydrogen adsorbed on bridge oxygen ($\text{Si}-\text{O}-\text{Si}$), and CH_2O^* intermediates, respectively.

NMR, the molar ratio of the spilt-over hydrogen at 773 K to the adsorbed CH_4 is about 1. This finding indicates that the undetected species of CH_x^* is reasonably deduced into CH_3^* . Furthermore, a new peak around 4.2 ppm appears. After the dry reforming reaction happens at 873 K, the intensity of the peaks around 1.0 ppm and 1.4 ppm greatly enhances, whereas the signal of H adsorbed on $\text{Si}-\text{O}-\text{Si}$ decreases obviously, suggesting the further interaction between the adsorbed H species and $\text{Si}-\text{O}-\text{Si}$ leads to the formation of $\text{Si}-\text{OH}$ group [51,53,55]. To assign the chemical shifts at 4.2 ppm and newly appeared at 4.7 ppm, different reagents of water, methanol, and formaldehyde were introduced into Rh/MCF system (Table 2). According to the intermediates detected previously in these systems [3,46], the peak around 4.7 ppm is attributed to CH_2O^* adsorbed species and that of 4.2 ppm to CH_3O^* adsorbed species [53,71]. When the temperature rises to 973 K, the intensity of CH_3O^* and CH_2O^* increases and dry reforming reaction takes place, whereas the intensity of $\text{Si}-\text{OH}$ decreases due to hydrogen desorption.

3.6. The proposed mechanism

In the temperature range of 298–773 K, the dry reforming reaction does not start. When the temperature increases to 673 K, carbon exchange reaction between CH_4 and CO_2 happens similarly as we illustrated in the previous report [53], and the spilt-over hydrogen from CH_4 decomposition mostly adsorbs on $\text{Si}-\text{O}-\text{Si}$ of the support. Based on the quantitative analysis of ^{13}C and ^1H adsorbed on rhodium surface, CH_3^* would be the main dissociated species of CH_4 (step 1). Then, CH_3^* reacts with the oxygen atom from CO_2 dissociation and forms CH_3O^* on rhodium surface at 773 K (step 2):

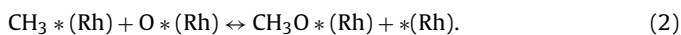
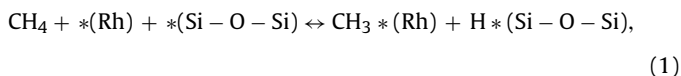
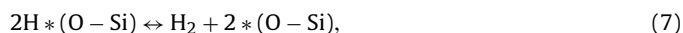
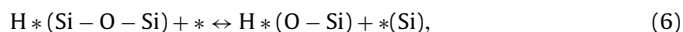
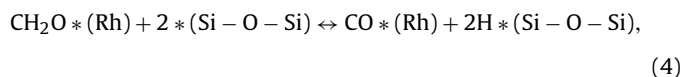
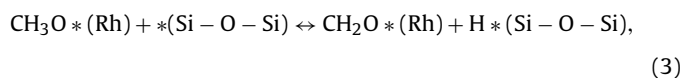


Table 2
Assignment of ^1H MAS NMR spectra of different reagents adsorbed over 1.0 wt% Rh/MCF.

Reagent added	Chemical shift (ppm)	
	—OH	—CH _x ($x=2-3$)
H_2O	3.1	—
CH_3OH	1.7	3.5 ($x=3$)
CH_2O	—	4.6 ($x=2$)

When the temperature is in the range of 873–973 K, the CH_2O^* (step 3) forms and the dry reforming reaction starts (steps 4–7) [3,46,53].



where $*(\text{Rh})$ represents the active centers on rhodium surface, $*(\text{Si}-\text{O}-\text{Si})$ and $*(\text{O}-\text{Si})$ represent the different oxygen sites of the support and $*(\text{Si})$ represents the oxygen vacancy sites of the silica, respectively.

In the above mechanism, the hydrogen atom from CH_4 dissociation (step 1) and the intermediates of CH_xO^* decomposition (step 3,4) can be split over to the vicinity of the bridge oxygen sites of $\text{Si}-\text{O}-\text{Si}$ on the support (step 1,3,4) but not at the metal–support interface for the little Knight shift effect from metal surface [66] and then reacts with $\text{Si}-\text{O}-\text{Si}$ to form $\text{H}^*(\text{O}-\text{Si})$ sites at the high temperature (step 6). Therefore, hydrogen spillover facilitates the dehydrogenation of the adsorbed intermediates on rhodium surface which can promote the reaction rate of dry reforming.

According to the literatures [15–23], hydrogen spillover is applied to the transportation of the hydrogen species formed on one phase to another phase. The phase generating hydrogen species is called the initiator, while the phase providing sites for the adsorption of hydrogen species is known as the acceptor. The obstacle in hydrogen spilling over mainly comes from the interface formed between the initiator and the acceptor. To reduce this limitation, three modifying methods were adopted in the solid preparation. Firstly, the highly dispersed metal species with small and “electronic-deficient” particle [72] were introduced as the active initiator to anchor tightly with the acceptor [24–26,31,32,]. Thus, the spilt-over hydrogen can be transferred easily and the hydrogen storage, hydrogenation, and dehydrogenation reaction were enhanced. Secondly, the support materials were required for accepting hydrogen atom [20]. Silica was reported to behave as the acceptor of spilt-over hydrogen due to its bridge oxygen sites [69,70]. Mesoporous silicas with high thermal stability and large surface area such as HMS and SBA-15 were used as the support in the reaction related with hydrogenolysis and dehydrogenation and was found to accept the spilt-over hydrogen from the initiator of metal species in the reaction process [19,53]. Lastly, some promoting agents were added to enhance the dispersion of loading metal. The addition species, including Ni, Ru, B, and Ca, were used to modify the surface of the active centers [28,33–36]. After that, the anchored intimacy between metal and support was formed as a bridge for the hydrogen spilling over [37,38,73]. Through the interface, the spilt-over hydrogen influences the formation rate of the intermediates and attends the hydrogenation and dehydrogenation process [42,43,74]. When the related step, e.g., the dehydrogenation step plays the dominant role of the redox reaction system [43], the reaction rate can be accelerated by the hydrogen spillover. For Rh/MCF with low metal content, rhodium species is highly dispersed on the foam-like silica, which leads to tight anchor between the initiator and the acceptor [15,20]. Therefore, in the reforming process hydrogen species from the steps of CH_4 dissociation and CH_3O^* and CH_2O^* intermediates decomposition on metal surface can be spilt over to the bridged oxygen acceptor of MCF easily through the formed interface [15,20,21,53]. This

simultaneous information on both the initiator and the acceptor can be obtained readily by controlled atmosphere MAS NMR measurements. The catalytic activity was greatly promoted by facilitating the steps (1,3,4) which were considered as the determining ones in dry reforming [3,4,46].

4. Conclusion

The promotional effect of hydrogen spillover was investigated in the methane dry reforming reaction over Rh/MCF. Strong hydrogen spillover occurs on Rh/MCF with high rhodium dispersion through H₂-TPD analysis. In the reforming reaction, TOF(CH₄) increases with the strength increment of spilt-over hydrogen over Rh/MCF. Controlled atmosphere ¹H and ¹³C MAS NMR disclosed that the hydrogen species from the steps of CH₄ dissociation and CH₃O* and CH₂O* intermediates decomposition can be spilt over to neighboring bridged oxygen sites of MCF and form surface terminal silanol groups. It is believed that hydrogen spillover can promote the reaction rate through facilitating the rate determining steps of CH₄ dissociation and the intermediates of CH_xO* (x = 2,3) decomposition in the reforming process.

Acknowledgements

This work was supported by the National Natural Science Foundation (21003024, 21173050, 21371035).

Appendix A. Supplementary data

Supplementary data associated with this article can be found, in the online version, at <http://dx.doi.org/10.1016/j.apcatb.2014.09.006>.

References

- [1] T.A. Chubb, Sol. Energy 24 (1980) 341–345.
- [2] J.R. Rostrupnielsen, J.H.B. Hansen, J. Catal. 144 (1993) 38–49.
- [3] M.C.J. Bradford, M.A. Vannice, Catal. Rev. Sci. Eng. 41 (1999) 1–42.
- [4] J.M. Wei, E. Iglesia, J. Catal. 225 (2004) 116–127.
- [5] L.P. Qian, B. Yue, S.P. Pei, L. Zhang, L. Ye, J.F. Cheng, S.C. Tsang, H.Y. He, Chin. J. Chem. 28 (2010) 1864–1870.
- [6] Z.L. Zhang, V.A. Tsiporiari, A.M. Efstathiou, X.E. Verykios, J. Catal. 158 (1996) 51–63.
- [7] S.H. Zeng, X.H. Zhang, X.J. Fu, L. Zhang, H.Q. Su, H. Pan, Appl. Catal. B: Environ. 136–137 (2013) 308–316.
- [8] Z.C. Liu, J. Zhou, K. Cao, W.M. Yang, H.X. Gao, Y.D. Wang, H.X. Li, Appl. Catal. B: Environ. 125 (2012) 324–330.
- [9] M.S. Fan, A.Z. Abdullah, S. Bhatia, Appl. Catal. B: Environ. 100 (2010) 365–377.
- [10] C.K. Shi, P. Zhang, Appl. Catal. B: Environ. 115–116 (2012) 190–200.
- [11] M.H. Amin, K. Mantri, J. Newham, J. Tardio, S.K. Bhargava, Appl. Catal. B: Environ. 119–120 (2012) 217–226.
- [12] D.P. Liu, X.Y. Quek, W.N.E. Cheo, R. Lau, A. Borgna, Y.H. Yang, J. Catal. 266 (2009) 380–390.
- [13] L.L. Xu, H.L. Song, L.J. Chou, Appl. Catal. B: Environ. 108–109 (2011) 177–190.
- [14] M.C.J. Bradford, M.A. Vannice, Catal. Today 50 (1999) 87–96.
- [15] W.C. Conner, J.L. Falconer, Chem. Rev. 95 (1995) 759–788.
- [16] S. Zhang, M.B. Katz, K. Sun, O.K. Ezekoye, M.I. Nandasiri, H.W. Jen, G.W. Graham, X.Q. Pan, J. Catal. 300 (2013) 201–204.
- [17] F. Benseradj, F. Sadi, M. Chater, Appl. Catal. A: Gen. 228 (2002) 135–144.
- [18] W.W. Lin, H.Y. Cheng, L.M. He, Y.C. Yu, F.Y. Zhao, J. Catal. 303 (2013) 110–116.
- [19] J.X. Chen, J.J. Zhou, R.J. Wang, J.Y. Zhang, Ind. Eng. Chem. Res. 48 (2009) 3802–3811.
- [20] V.V. Rozanov, O.V. Krylov, Russ. Chem. Rev. 66 (1997) 107–119.
- [21] J.T. Miller, B.L. Meyers, F.S. Modica, G.S. Lane, M. Vaarkamp, D.C. Koningsberger, J. Catal. 143 (1993) 395–408.
- [22] S.X. Xia, R.F. Nie, X.Y. Lu, L.N. Wang, P. Chen, Z.Y. Hou, J. Catal. 296 (2012) 1–11.
- [23] N.Z. Zhang, K.S. Rama Rao, M.J. Jin, S.E. Park, Appl. Catal. A: Gen. 425–426 (2012) 62–67.
- [24] C.H. Chen, M.S. Yu, C.S. Tsao, H.Y. Chuang, H.H. Tseng, T.Y. Chung, Micropor. Mesopor. Mater. 152 (2012) 157–162.
- [25] V.B. Parambath, R. Nagar, K. Sethupathi, S. Ramaprabhu, J. Phys. Chem. C 115 (2011) 15679–15685.
- [26] H. Zhou, X.Q. Liu, J. Zhang, X.F. Yan, Y.J. Liu, A.H. Yuan, Int. J. Hydrogen Energy 39 (2014) 2160–2167.
- [27] P. Dibandjo, C. Zlotea, R. Gadiou, C.M. Ghimbeu, F. Cuevas, M. Latroche, E. Leroy, C. Vix-Guterl, Int. J. Hydrogen Energy 38 (2013) 952–965.
- [28] Y. Wang, K. Wang, C. Guan, Z.M. He, Z.S. Lu, T. Chen, J. Liu, X. Tan, T.T.Y. Tan, C.M. Li, Int. J. Hydrogen Energy 36 (2011) 13663–13668.
- [29] C.C. Huang, N.W. Pu, C.A. Wang, J.C. Huang, Y. Sung, M.D. Ger, Sep. Purif. Technol. 82 (2011) 210–215.
- [30] S. McArdle, T. Curtin, J.J. Leahy, Appl. Catal. A 382 (2010) 332–338.
- [31] X. Wang, N. Perret, J.J. Delgado, G. Blanco, X. Chen, C.M. Olmos, S. Bernal, M.A. Keane, J. Phys. Chem. C 117 (2013) 994–1005.
- [32] M. Chettibi, A.G. Boudjahem, M. Bettahar, Trans. Metal Chem. 36 (2011) 163–169.
- [33] J.H. Lee, S.K. Kim, I.Y. Ahn, W.J. Kim, S.H. Moon, Korea. J. Chem. Eng. 29 (2012) 169–172.
- [34] J.J. Liu, L.L. Zhang, J.T. Zhang, T. Liu, X.S. Zhao, Nanoscale 5 (2013) 11044–11050.
- [35] J.F. Yu, Q.J. Ge, W. Fang, H.Y. Xu, Int. J. Hydrogen Energy 36 (2011) 11536–11544.
- [36] J.N.G. Stanley, K. Worthington, F. Heinroth, A.F. Masters, T. Maschmeyer, Catal. Today 178 (2011) 164–171.
- [37] P. Weerachawanasak, P. Praserttham, J. Panpranot, J. Nanosci. Nanotechnol. 14 (2014) 3170–3175.
- [38] R.J. Shi, F. Wang, Tana, Y. Li, X.M. Huang, W.J. Shen, Green Chem. 12 (2010) 108–113.
- [39] X.H. Lin, K. Yang, R.R. Si, X. Chen, W.X. Dai, X.Z. Fu, Appl. Catal. B: Environ. 147 (2014) 585–591.
- [40] B.T. Meshesha, N. Barrabes, K. Fotthinger, R.J. Chimentao, J. Llorca, F. Medina, G. Rupprechter, J.E. Sueiras, Appl. Catal. B: Environ. 117–118 (2012) 236–245.
- [41] N.S. Babu, N. Lingaiah, P.S.S. Prasad, Appl. Catal. B: Environ. 111–112 (2012) 309–316.
- [42] S.E. Collins, J.J. Delgado, C. Mira, J.J. Calvino, S. Bernal, D.L. Chiavassa, M.A. Baltanas, A.L. Bonivardi, J. Catal. 292 (2012) 90–98.
- [43] C. Nederlof, G. Talay, F. Kapteijn, M. Makkee, Appl. Catal. A: Gen. 423 (2012) 59–68.
- [44] R.N. Bhat, W.M.H. Sachtler, Appl. Catal. A: Gen. 150 (1997) 279–296.
- [45] M.F. Mark, W.F. Maier, Angew. Chem. Int. Ed. 33 (1994) 1657–1660.
- [46] M.C.J. Bradford, M.A. Vannice, Appl. Catal. A: Gen. 142 (1996) 97–122.
- [47] K. Walter, O.V. Buyevskaya, D. Wolf, M. Baerns, Catal. Lett. 29 (1994) 261–270.
- [48] L.P. Qian, Z. Ma, Y. Ren, H.C. Shi, B. Yue, S.J. Feng, J.Z. Shen, S.H. Xie, Fuel 122 (2014) 47–53.
- [49] E.G. Karpov, M.A. Hashemian, S.K. Dasari, J. Phys. Chem. C 117 (2013) 15632–15638.
- [50] Y. Lykhach, T. Staudt, M. Vorokhta, T. Skala, V. Johaneck, K.C. Prince, V. Matolin, J. Libuda, J. Catal. 285 (2012) 6–9.
- [51] M. Wallin, H. Gronbeck, A.L. Spetz, M. Eriksson, M. Skoglundh, J. Phys. Chem. B 109 (2005) 9581–9588.
- [52] M.W. Anderson, J. Klinowski, Nature 339 (1989) 200–203.
- [53] L.P. Qian, Y. Ren, H. Yu, Y. Wang, B. Yue, H.Y. He, Appl. Catal. A: Gen. 401 (2011) 114–118.
- [54] L. Zhang, Y.H. Ren, B. Yue, H.Y. He, Chem. Commun. 48 (2012) 2370–2384.
- [55] T.H. Wu, D.M. Lin, Y. Wu, X.P. Zhou, Q.G. Yan, W.Z. Weng, H.L. Wan, J. Nat. Gas Chem. 16 (2007) 316–321.
- [56] P. Schmidt-Winkel, W.W. Lukens, P.D. Yang, D.I. Margolese, J.S. Lettow, J.Y. Ying, G.D. Stucky, Chem. Mater. 12 (2000) 686–696.
- [57] P. Schmidt-Winkel, W.W. Lukens, D.Y. Zhao, P.D. Yang, B.F. Chmelka, G.D. Stucky, J. Am. Chem. Soc. 121 (1999) 254–255.
- [58] J.L. Liu, L.J. Zhu, Y. Pei, J.H. Zhuang, H. Li, H.X. Li, M.H. Qiao, K.N. Fan, Appl. Catal. A 353 (2009) 282–287.
- [59] H. Kusama, K. Okabe, K. Sayama, H. Arakawa, Appl. Organomet. Chem. 14 (2000) 836–840.
- [60] P. Panagiotopoulou, D.I. Kondarides, Appl. Catal. B: Environ. 101 (2011) 738–746.
- [61] S.S. Kim, H.H. Lee, S.C. Hong, Appl. Catal. B: Environ. 119–120 (2012) 100–108.
- [62] C. Dall'Agnol, A. Gervasini, F. Morazzoni, F. Pinna, G. Strukul, L. Zanderighi, J. Catal. 96 (1985) 106–114.
- [63] P.M. Mortensen, J.D. Grunwaldt, P.A. Jensen, A.D. Jensen, ACS Catal. 3 (2013) 1774–1785.
- [64] M.L. Zhang, S.F. Ji, L.H. Hu, F.X. Yin, C.Y. Li, H. Liu, Chin. J. Catal. 27 (2006) 777–782.
- [65] L.P. Qian, Y. Cao, B. Yue, Y. Ren, B.L. Chen, H.Y. He, Chin. J. Catal. 26 (2005) 455–457.
- [66] K. Tedsree, A.T.S. Kong, S.C. Tsang, Angew. Chem. Int. Ed. 48 (2009) 1443–1446.
- [67] M. Hunger, Catal. Rev. Sci. Eng. 39 (1997) 345–393.
- [68] D. Ma, Y.Y. Shu, W.P. Zhang, X.W. Han, Y.D. Xu, X.H. Bao, Angew. Chem. Int. Ed. 39 (2000) 2928–2931.
- [69] Z.S. Chao, T.H. Wu, J.L. Ye, G.Z. Chen, H.L. Wan, Sci. Chin. Ser. B: Chem 44 (2001) 103–112.
- [70] T.H. Wu, Q.G. Yan, Q.N. Zhang, Z.J. Niu, Z.S. Chao, J.L. Ye, H.L. Wan, Chin. J. Catal. 25 (2004) 909–914.
- [71] H.A. Szymanski, R.E. Yelini, NMR Band Handbook, IFI/Plenum Data Corp., New York, NY, 1968.
- [72] X. Li, F. Zhou, A.J. Wang, L.Y. Wang, Y. Wang, Energy Fuels 26 (2012) 4671–4679.
- [73] J.A. Cecilia, I. Jimenez-Morales, A. Infantes-Molina, E. Rodriguez-Castellon, A. Jimenez-Lopez, J. Mol. Catal. A 368 (2013) 78–87.
- [74] M.V. Dementyeva, T.F. Sheshko, Y.M. Serov, Theor. Exp. Chem. 49 (2013) 46–51.